Morphological changes in intracellular lipid droplets induced by different hepatitis C virus genotype core sequences and relationship with steatosis.

Aurélie Piodi, Philippe Chouteau, Hervé Lerat, Christophe Hézode, Jean-Michel Pawlotsky

Morphological Changes in Intracellular Lipid Droplets Induced by Different Hepatitis C Virus Genotype Core Sequences and Relationship with Steatosis

Aurélie Piodi,[1,2]* Philippe Chouteau,[1,2]* Hervé Lerat,[1,2] Christophe Hézode,[1,2,3] and Jean-Michel Pawlotsky[1,2]

[1]French National Reference Center for Viral Hepatitis B, C and delta, Department of Virology, Hôpital Henri Mondor, Université Paris 12; [2]INSERM U841; and [3]Department of Hepatology and Gastroenterology, Hôpital Henri Mondor, Université Paris 12, Créteil, France

*These two authors participated equally in the study

Key words: hepatitis C virus, steatosis, lipid droplets, core protein, colocalization

FOOTNOTE PAGE

Corresponding author: Prof. Jean-Michel PAWLOTSKY, MD, PhD, Department of Virology, Hôpital Henri Mondor, 51 avenue du Maréchal de Lattre de Tassigny, 94010 Créteil, France

Tel: +33-1-4981-2827; Fax: +33-1-4981-4831

E-mail: jean-michel.pawlotsky@hmn.aphp.fr

Abbreviations: HCV: hepatitis C virus; BMI: body mass index; HOMA: Homeostasis Model Assessment; NAFLD: non-alcoholic fatty liver disease; PCR: polymerase chain reaction; FCS: fetal calf serum; mAb: monoclonal antibody; CCF: cross-correlation function; SEM: standar error of the mean; CI: confidence interval; FAS: fatty acid synthase; SREBP: sterol regulatory element binding protein;

Financial support: This work was supported by grants from Agence Nationale de Recherche sur le SIDA et les Hépatites Virales (ANRS) and Agence Nationale de la Recherche (ANR, Grant ANR-05-PCOD-035-01). A.P. was supported by fellowships from the French Ministry of Research and ANRS.

ABSTRACT

Hepatocellular steatosis is common in patients with chronic hepatitis C. Steatosis can be considered as a true cytopathic lesion induced by hepatitis C virus genotype 3, suggesting that one or more viral proteins produced during genotype 3 infection are involved in the steatogenic process, while the same proteins produced during infection by other genotypes are not. We examined *in vitro* interactions between lipid droplets and full-length core protein isolated from patients with hepatitis C virus genotype 3a infection, with and without steatosis, and from steatosis-free patients infected by hepatitis C virus genotype 1b. We also examined morphological changes in the lipid droplets according to the hepatitis C virus genotype and the presence of steatosis *in vivo*. Core protein processing by signal peptide peptidase was not affected by sequence differences between the variants. We showed that the core protein of both hepatitis C virus genotypes 1b and 3a binds tightly to the surface of intracellular lipid droplets. However, cells transfected with genotype 3a contain more neutral lipids in lipid droplets, and more large lipid droplets, than cells transfected with genotype 1b sequences. This suggests that hepatitis C virus core protein-lipid droplet interaction could play a role in virus-induced steatosis. Importantly, we found no genetic or functional differences between genotype 3a core proteins from patients with and without hepatitis C virus-induced steatosis. This suggests that other viral proteins and/or host factors are involved in the development of hepatocellular steatosis in patients infected by hepatitis C virus genotype 3a.

Hepatocellular steatosis (triglyceride accumulation in the hepatocyte cytoplasm) is a common histological finding in patients with chronic hepatitis C virus (HCV) infection. Steatosis is a cofactor for fibrosis and disease progression in chronic hepatitis C (1-6). Various metabolic parameters are associated with the onset and severity of steatosis regardless of the HCV genotype, including the body mass index (BMI), hyperlipidemia, type 2 diabetes and insulin resistance (2-5, 7-19). Moreover, HCV genotype 3 is independently associated with hepatocellular steatosis, which can thus be considered as a true cytopathic lesion induced by this HCV genotype (3-13, 17, 20-22). This suggests that one or more viral proteins produced during genotype 3 infection are involved in the steatogenic process, while the same proteins produced during infection by other genotypes are not.

Experimental studies have shown complex interactions between HCV core protein, lipids and lipid metabolism. In particular, HCV core protein can induce intracellular accumulation of lipids, both in cell culture and in transgenic mice (20, 23-30). In cell culture, HCV core protein associates with cytoplasmic lipid droplets, lipid storage organelles rich in cholesterol esters and in di- and triacylglycerol (23, 31-33). This interaction was recently suggested to involve HCV core protein domain D2, that spans amino acids 118-173 and contains two amphipathic α-helices that likely associate in-plane at the lipid droplet membrane layer interface (32, 34, 35).

Most experimental studies published to date have focused on sequences derived from HCV genotype 1, which is not associated with steatosis. HCV genotype 3 core protein expression has been reported to induce stronger intracellular lipid accumulation *in vitro* than genotype 1 core protein expression (26, 36), apparently as

the result of a single amino acid difference in the D2 domain (36). None of these reports mentioned whether or not the patients from whom the core sequences were isolated had steatosis.

Here we examined *in vitro* interactions between lipid droplets and full-length core protein isolated from patients with HCV genotype 3a infection, with and without steatosis, and from steatosis-free patients infected by HCV genotype 1b. We also examined morphological changes in the lipid droplets according to the HCV genotype and the presence of steatosis *in vivo*.

MATERIALS AND METHODS

Materials

The patients were selected from our institutional database of HCV-infected patients, based on the following criteria: (i) chronic HCV infection, confirmed by the presence of serum anti-HCV antibodies (Ortho^{TM} HCV 3.0 Elisa Test System, Ortho-Clinical Diagnostics, Raritan, New Jersey) and HCV RNA (Amplicor HCV 2.0 PCR Test System, Roche Molecular Systems, Pleasanton, California); (ii) HCV genotype 1b or 3a infection, as suggested by a line probe assay (INNO-LiPA HCV II, Innogenetics, Gent, Belgium) and confirmed by sequence determination and phylogenetic analysis of a portion of the NS5B region; (iii) histologically proven chronic hepatitis; (iv) no previous or current antiviral therapy; and (v) no coinfection with hepatitis B virus or human immunodeficiency virus.

All the patients had had a liver biopsy. The specimens were fixed in formalin and paraffin sections were stained with hematoxylin-eosin-safran for analysis by a

pathologist. Fibrosis and inflammation were graded with the METAVIR system. Steatosis was graded as absent (0 or < 1% of affected hepatocytes, grade 0), mild (1% to 10% of affected hepatocytes, grade 1), moderate (10% to 30% of affected hepatocytes, grade 2) or marked (> 30% of affected hepatocytes, grade 3). Patients were considered to have HCV-induced steatosis only if they had moderate or marked histological steatosis at baseline and a reduction of at least two grades on repeat biopsy after successful antiviral therapy. Steatosis-free patients all had grade 0 steatosis. In order to eliminate patients with metabolic causes of steatosis, we also applied the following selection criteria: (i) mean alcohol intake within the 6 months preceding liver biopsy < 20 g/day; (ii) body mass index (BMI) < 27 kg/m^2; (iii) baseline serum glucose level < 6.1 mmol/L; (iv) serum fasting triglycerides < 1.7 mmol/L; (v) cholesterol < 6.1 mmol/L; (vi) Homeostasis Model Assessment (HOMA) index of insulin resistance < 2.4; and (vii) no diabetes or known metabolic risk factors for non-alcoholic fatty liver disease (NAFLD).

Eight patients were selected for this study, comprising five patients infected by HCV genotype 3a (of whom three had HCV-induced steatosis), and three steatosis-free patients infected by genotype 1b. Their characteristics are shown in Table 1. HCV RNA was extracted from their serum and the full-length core protein-coding sequence was amplified by means of reverse transcriptase polymerase chain reaction (PCR).

Methods

HCV RNA extraction and cDNA synthesis. HCV RNA was extracted from 200 µl of serum with the High Pure viral RNA kit (Roche Applied Science,

Indianapolis, Indiana), according to the manufacturer's instructions. Viral RNA was recovered in 50 µl of RNase-free water and stored at -80°C until being processed. Five microliters of the extracted viral RNA was reverse-transcribed for 60 min at 50°C using 0.5 mM each dNTP, 10 pmol of random hexamers, 10 mM DTT, 40 U of RNase OUT and 200 U of Superscript III reverse transcriptase (Invitrogen, Carlsbad, California). The samples were heated for 15 min at 70°C to stop the reaction and were frozen until processed.

PCR amplification and cloning. It has been shown that expression of the full-length core sequence alone (amino acids 1 to 191) is associated with incomplete cellular translocation (37). To ensure correct processing, at least the first 100 amino acids of E1 are required for the construction of expression vectors. A sequence spanning the full-length core-coding region and the first 400 nucleotides coding for the E1 envelope glycoprotein (core-ΔE1 sequence) was amplified by means of a nested PCR procedure using genotype-specific primers (Table 2). Restriction sites were included in the second-round primers for the cloning procedure. In order to characterize the quasispecies distribution of HCV proteins, purified PCR products were cloned in the pHM6 vector (Roche Applied Sciences) and 20 clones per sample were generated. Core-ΔE1 quasispecies variant sequences were determined with the ABI PRISM BigDye Terminator Cycle Sequencing Ready Reaction kit on an ABI PRISM 377 DNA Sequencer (Applied Biosystems, Foster City, California). Plasmids containing the most frequent core-ΔE1 quasispecies variant sequence from each of the eight chronically infected patients shown in Table 1 were designated pCΔE1-1b/1NS, pCΔE1-1b/2NS, pCΔE1-1b/3NS, pCΔE1-3a/1NS, pCΔE1-3a/2NS, pCΔE1-

3a/1S, pCΔE1-3a/2S, pCΔE1-3a/3S for patients 1b-1NS, 1b-2NS, 1b-3NS, 3a-1NS, 3a-2NS, 3a-1S, 3a-2S, and 3a-3S, respectively.

Core-ΔE1 expression in Huh7 cells. Huh7 human hepatoma cells were grown in the presence of 5% CO_2 in Dulbecco's Modified Medium containing 4500 mg/mL glucose (Invitrogen) and supplemented with 10% fetal calf serum (FCS), antibiotics (4.5 mg/L penicillin, 50 mg/L streptomycin), 5 mg/L insulin and 3.5 x 10^{-7} M hydrocortisone hemisuccinate. Cells were electroporated (Nucleofection™, Amaxa, Köln, Germany) with 4 µg of plasmid for 4 million cells. One million cells were cultured on slides (4-well Lab-Tek II chamber slide system, Nalge Nunc Int., Rochester, New York) for core protein immunostaining and lipid droplet analysis, and the remaining 3 million cells were cultured in 6-well plates for western-blot and lipid analyses. Cells were cultured for 24 h in the presence of 5% CO_2 in Dulbecco's Modified Medium containing 1000 mg/mL glucose supplemented with 10% FCS and antibiotics (4.5 mg/L penicillin, 50 mg/L streptomycin).

Assessment of core protein processing by signal peptide peptidase. BHK cells were used to test HCV core protein processing by signal peptide peptidase (SPP). BHK C13 cells were grown in the presence of 5% CO_2 in MEM Eagle with 2 mM L-glutamine (Invitrogen) supplemented with 10% FCS, 100µM Non Essential Amino Acid (Invitrogen) and 10µM sodium pyruvate (Invitrogen). Cells were transfected with the different core protein sequences with Lipofectamine LTX (Invitrogen), according to the manufacter's instructions. When necessary, cells were incubated with 100 µM of the SPP inhibitor $(Z\text{-}LL)_2$ ketone immediately following transfection. After incubation for 16 h, cells were harvested and washed twice in phosphate buffered saline (PBS)

containing 10 mM EDTA, 0.5% NP40 and anti-proteases. A crude total protein extract was obtained by multiple freezing and thawing steps. For western-blot analysis, proteins were separated by SDS-PAGE using 12% Tris-Glycine gels (Bio-Rad, Hercules, California), transferred onto nitrocellulose membranes, and probed with an HRP-conjugated rat anti-HA MAb. (3F10, Roche Applied Sciences). The HA-tagged core protein was detected by means of enhanced chemiluminescence.

Indirect immunofluorescence and lipid staining. Indirect immunofluorescence and lipid staining experiments were performed in both core protein-transfected Huh7 cells and Huh7 cells infected with JFH1 viral particles (kindly provided by Dr Jean Dubuisson) (38-40). For the latter experiment, Huh7.5 cells were electroporated with an RNA transcribed from the HCV genotype 2a JFH1 plasmid, grown for two successive passages for approximately 20 days, and their supernatants were applied to naïve Huh7 cells. Cells grown on slides were washed three times with PBS and fixed for 10 min in 4% paraformaldehyde. After two washes with PBS the cells were incubated for 40 min in PBS containing 0.3% bovine serum albumin and 0.1% saponin. The cells were then immunolabeled with either the anti-HCV core monoclonal antibody (mAb) Acap27 (Bio-Rad, Hercules, California) at 1:1000 dilution, or an anti-HA mAb (Roche Applied Sciences) at 1:25 dilution. Anti-HCV core staining was visualized with TRITC-conjugated goat anti-mouse IgG (Sigma-Aldrich, Saint-Louis, Missouri), and lipid droplet association was studied by using the BODIPY 493/503 fluorophore (10 µg/ml, Molecular Probes, Eugene, Oregon). Anti-HA staining was visualized with Alexa 694-conjugated goat anti-rat IgG at 1:400 dilution (Invitrogen and Molecular Probes) and lipid droplet association was studied with an anti-ADRP mAb at 1:2 dilution (Progen, Heidelberg, Germany) and

visualized with FITC-conjugated goat anti-mouse IgG (Bio-Rad). The slides were washed in PBS and mounted in fluorescent mounting medium containing DAPI (Vectashield, Vector Laboratories, Burlingame, California).

Lipid droplet morphometry and colocalization studies. The spatial location of core protein and lipid droplets in Huh7 cells was studied by means of confocal laser scanning microscopy with a Leica DMRE-7/TCS-SP2 device (Leica, Wetzlar, Germany). A 405-nm diode laser, a 488-nm line of an argon-ion laser, a 543-nm line of a helium-neon laser and a 594-nm line of a helium-neon laser were to excite Dapi, Bodipy 493/503 and FITC, TRITC and Alexa 594, respectively. 3D visualization of lipid droplets, with and without core protein, was performed after double-labeling with anti-core mAb and Bodipy 493/503. Z-stacks of serial 0.3-µm-thick confocal sections were acquired separately for each channel to exclude cross-talk between channels due to the partly overlapping emission spectra of the dyes. Image processing and 3D reconstruction were performed with the Imaris software package (Bitplane AG, Zürich, Switzerland). The largest diameter of each reconstructed lipid droplet was exposed by rotating stack and was measured manually in the image graphics plane.

To study the colocalization of core protein and ADRP, single optical slices were recorded separately in each dye-corresponding channel in double-labeled cells. Colocalization was assessed by statistical analysis of the correlation of the intensity values of red (core protein) and green (ADRP) pixels in a dual-channel image. JACoP plugging from ImageJ software was used to calculate Pearson's correlation coefficient, to visualize scatter plots, and to perform cross-correlation analysis (Van Steensel's cross-correlation function). Pearson's coefficient-based analysis results in a pixel distribution diagram (scatter plot), where the intensity of a given pixel in the

green image is used as the x-coordinate and the intensity of the corresponding pixel in the red image as the y-coordinate. In a colocalization situation, dots on the diagram appear as a cloud centered on a line. The spread of this distribution with respect to the fitted line can be estimated by calculating the correlation coefficient, also called Pearson's coefficient (R). A cross-correlation function (CCF) reveals differences in intensity pixels through the value of the maximum peak of the bell-shaped curve and allows partial colocalization events to be discriminated through the deviation from 0 (pixel shift: dx) and/or the presence of peaks aside dx.

Statistical analysis. The results are reported as the mean ± standard error of the mean (SEM). Student's *t* test was used for parametric variables and the Wilcoxon test for nonparametric variables. P values of < 0.05 were considered significant.

RESULTS

Patient selection. The eight selected patients (Table 1) belonged to three groups based on their HCV genotype (3a or 1b) and the presence (S) or absence (NS) of steatosis on liver biopsy prior to any therapy. Three patients (Group A, patients 3a-1S to 3a-3S) were infected by HCV genotype 3a and had marked or severe HCV-induced steatosis, according to the criteria described in Methods; two patients (Group B, patients 3a-1NS and 3a-2NS) were infected by HCV genotype 3a and had no steatosis on liver biopsy; and three patients (Group C, patients 1b-1NS to 1b-3NS) were infected by HCV genotype 1b and had no steatosis on liver biopsy (Table 1). It should be noted that none of the patients had both genotype 1b infection and HCV-induced steatosis. Mean HCV RNA levels did not differ significantly among

the three groups.

Relationship between core-ΔE1 sequences (quasispecies analysis), the HCV genotype, and steatosis. In order to ensure correct processing of the experimentally expressed core protein, a sequence spanning the full-length core-coding region from each of the eight patients, plus the first 400 nucleotides coding for the E1 envelope glycoprotein, was PCR-amplified. The PCR products were cloned and 20 clones per sample were sequenced in order to determine the quasispecies distribution of core sequences. As shown in Figure 1A, genotype-specific amino acid differences were observed between the genotype 1b and 3a sequences. Among the patients infected by HCV genotype 3a, only a few single amino acid differences were observed, and these differences were not related to the presence or absence of steatosis *in vivo* (Figure 1A). The amino acid repertoires deduced by aligning the quasispecies variants from genotype 3a-infected patients did not differ with respect to the presence or absence of steatosis, except, possibly, at position 16, where a difference in amino acid frequencies was observed between the two groups (Figure 1B). Overall, we found no motifs or amino acids specifically associated with the presence or absence of steatosis in the core sequences isolated from patients infected by HCV genotype 3a.

Expression of core-ΔE1 sequences and interaction with lipid droplets. The most frequent core-ΔE1 variant sequences from each patient's quasispecies were cloned in fusion with an HA tag and a 6xHIS tag at their amino- and carboxy-termini, respectively. In order to evaluate potential differences in the processing of different core proteins, we assessed SPP cleavage efficiency by means of $(Z\text{-}LL)_2$

ketone, an SPP inhibitor. This experiment was performed in BHK cells because (Z-LL)$_2$ ketone has weaker SPP inhibition activity in Huh7 cells. The cleavage profiles of the different core proteins are shown in Figure 2. All constructs were fully processed by SPP. Indeed, in untreated cells, only the processed 21 kD form was present in all instances, whereas in (Z-LL)$_2$ ketone-treated cells, the uncleaved (23 kD) form of the core protein was also present (Figure 2).

The tagged Core-ΔE1 sequences were transfected into Huh7 cells and their expression was assessed by immunoblot and densitometric analysis 24 h later. Core-ΔE1 proteins originating from patients infected by HCV genotypes 1b and 3a, with and without steatosis, were equally expressed in transfected Huh7 cells (data not shown). Transfected Huh7 cells were then immuno-labeled for core protein, and lipid droplets were stained with BODIPY 493/503. Core-expressing Huh7 cells were analyzed individually by confocal fluorescence microscopy for core protein-lipid droplet association. Lipid droplets were reconstructed in 3D from optical section stacks. Figure 3A shows representative staining and spatial representations of 3D reconstructions in each group. In core-expressing cells, lipid droplets were surrounded by HCV core protein, regardless of the HCV genotype, and were principally localized in the perinuclear area. Lipid droplets were more evenly distributed in the cytoplasm of mock-transfected cells (data not shown). In order to confirm these observations in the context of an infectious genome, we analyzed the respective core protein and lipid droplet localizations in Huh7 cells infected by JFH1 viral particles produced in cell culture (Figure 3A, right panel). Like Huh7 cells transiently transfected with HCV core proteins, JFH1-infected cells showed an exclusive localization of core proteins at the surface of lipid droplets, that formed ring-like structures with a perinuclear localization.

Figure 3B shows a 3D representation of HCV core protein bound to the surface of intracytoplasmic lipid droplets. Importantly, in cells expressing HCV genotype 3a core protein, core protein-lipid droplet colocalization was independent of the presence or absence of steatosis in the corresponding patient.

Lipid droplet morphological changes induced by core-ΔE1 sequence expression. The number of lipid droplets per cell and their size were measured by confocal fluorescence microscopy. The cumulative volume of lipid droplets per core-expressing cell, *i.e.* the total amount of neutral lipids per cell, was measured (Figure 4A). Fifteen mock-transfected cells (control cells) were randomly selected, along with 65 cells expressing genotype 3a-S constructs from the three relevant patients, 48 cells expressing genotype 3a-NS constructs (two patients), and 66 cells expressing genotype 1b-NS constructs (three patients). The cumulative volume of lipid droplets was not significantly different between Huh7 cells transfected with HCV genotype 1b core protein and mock-transfected control cells (487±44 μm^3 *vs* 603±50 μm^3 neutral lipids/cell, respectively). In contrast, cells expressing genotype 3a core protein contained a significantly larger volume of lipid droplets than control cells and than cells expressing genotype 1b core protein ($p<0.0001$ and $p=0.001$, respectively). No difference was seen in genotype 3a core-expressing cells with respect to whether or not the corresponding patients had steatosis (1003±87 μm^3 *vs* 943±124 μm^3 neutral lipids/cell with genotype 3a core protein derived from patients with and without steatosis, respectively).

The diameters of 9147 individual lipid droplets was also calculated in transfected cells. In control cells the average diameter was 2.3 µm, and no lipid droplets had a diameter greater than 6 µm. We used this threshold to define “very

large" lipid droplets (> 6 µm). Figure 4B shows the proportion of very large lipid droplets in cells expressing genotype 1b and 3a core protein, according to the presence and absence of steatosis in vivo. Cells expressing genotype 1b core protein harbored a significantly larger number of very large lipid droplets than control cells (0.79%, 95% confidence interval (CI): 0.66%-1.12%; p=0.001). Moreover, very large lipid droplets were significantly more frequent in cells expressing genotype 3a core protein than in cells expressing genotype 1b core protein (p<0.0001). In contrast, no significant difference was observed in cells expressing HCV genotype 3a core protein with respect to steatosis: (2.45% (95%CI: 1.85%-3.05%) *vs* 2.85% (95%CI: 2.80%-2.90%) with genotype 3a core protein derived from patients with and without steatosis, respectively).

Overall, the expression of HCV genotype 1b core protein did not influence the total amount of intracellular neutral lipids associated with lipid droplets. In contrast, the expression of HCV genotype 3a core protein approximately doubled the amount of intracellular neutral lipids associated with lipid droplets. In addition, genotype 3a core protein expression was associated with a significantly higher proportion of large lipid droplets (> 6µm) in the cell cytoplasm as compared to mock-transfected control cells and to cells expressing genotype 1b core protein. Importantly, the larger amount of intracellular neutral lipids and the more frequent presence of very large lipid droplets associated with genotype 3a core expression was independent of steatosis.

Qualitative and quantitative analysis of HCV core protein-lipid droplet colocalization. We used confocal laser scanning microscopy to record single optical slices in each dye-corresponding channel in cells labeled for both HCV core protein and ADRP, a protein associated with the surface of intracellular lipid droplets. The

immunofluorescence patterns appeared as intracytoplasmic rings for both HCV core protein and ADRP (Figure 5). Merged images confirmed the tight and exclusive association of HCV genotype 1b and 3a core protein with the surface of lipid droplets (Figure 5). Genotype 3a core protein colocalization was not influenced by the steatotic status of the corresponding patients (Figure 5).

We also studied core protein-ADRP colocalization in lipid droplets of different sizes. As the mean diameter of lipid droplets was 2.3 µm, "large" droplets were defined as having a diameter of 2.3 µm or more, and "small" lipid droplets as having a diameter of less than 2.3 µm. Correlations between the intensities of red (core protein) and green (ADRP) pixels in dual-channel images were studied by using Pearson's coefficient (R) in several isolated lipid droplets obtained from cropped images in each study group. R-values indicated a high level of core-ADRP colocalization (average R-value: 0.885), whatever the genotype of origin of the core protein and the corresponding patients' steatotic status (data not shown). Figures 6A and 6B show representative results obtained with cells expressing genotype 1b, 3a-NS and 3a-S core protein. Despite slight differences in fluorescence intensity shown by the deflection of pixel distribution towards the red axis, the scatter plot dots accumulated around the diagonal for large lipid droplets (> 2.3 µm), but were more dispersed for small lipid droplets (< 2.3 µm), suggesting slightly weaker colocalization (Figure 6). Furthermore, the spread of dots was larger with genotype 1b than with genotype 3a core protein, also suggesting weaker colocalization with genotype 1b (Figure 6).

As shown in Figure 6C, which compares mean R-values in large and small lipid droplets for each core protein category, the R-values were always smaller for small lipid droplets than for large lipid droplets. However, the difference was

significant only for HCV genotype 1b sequences ($p<0.05$). Together, these data suggested weaker HCV core protein binding to small than large lipid droplets, a phenomenon that appeared to be more pronounced for HCV genotype 1b sequences. As a difference in pixel intensities in the two fluorescence channels could cause greater spread in the scatter plots, we also calculated Van Steensel's CCF. This revealed no major differences in pixel intensities ($CCF_{max} = 0.915 \pm 0.006$) and confirmed the correlation of red and green pixels ($dx = -0.6 \pm 0.1$). However, in analyses of small lipid droplets, the presence of peaks at the ends of the bell-shaped curve revealed excluded pixels (Figure 6).

DISCUSSION

We transfected Huh7 cells with HCV core protein sequences from steatosis-free patients infected by HCV genotype 1b, and from genotype 3a-infected patients with and without HCV-induced steatosis. We were thus able to study the relationship between the *in vivo* steatogenic properties of the viruses and the ability of their core proteins to associate with intracellular lipid droplets and to induce lipid accumulation. In order to ensure correct processing of the core protein, the full-length core protein sequence was expressed along with the first 400 nucleotides coding for the E1 envelope glycoprotein (37). SPP cleavage of the core protein, which is required for its localization to the surface of lipid droplets, was found to be equally efficient with all of the studied constructs.

We found similar HCV core protein binding to the lipid droplet surface, irrespective of the HCV genotype (1b and 3a) and, in genotype 3a-infected patients, independently of steatosis. Core protein binding was associated with an

accumulation of lipid droplets in the perinuclear area. Binding of HCV proteins to lipid droplets has previously been reported in cultured transfected cells (23, 26, 31-33, 36) and also recently in the JFH1-based productive HCV culture system, in which mature HCV core protein extensively colocalizes with lipid droplets, as confirmed here (41, 42). Our results indicate that HCV core protein can associate with lipid droplets regardless of the genotype and the *in vivo* steatogenic potency of the corresponding viral strain. They further suggest that core protein localization at the lipid droplet surface is not the only mechanism underlying HCV-induced steatosis, a complication associated mainly, if not exclusively, with genotype 3a infection.

We also found that, relative to genotype 1b core protein, intracellular expression of HCV genotype 3a core protein was associated with more marked accumulation of neutral lipids contained in lipid droplets and with larger lipid droplets, a result in keeping with a role of core protein-lipid droplet association in the onset of HCV genotype 3a-induced steatosis. Several authors have shown that HCV genotype 3a core protein interacts with lipid metabolism. In particular, it induces fatty acid synthase (FAS), an enzyme required for intracellular triglyceride production (43). Another study has shown that HCV core protein, and other HCV proteins, can induce the cleavage of sterol regulatory element binding proteins (SREBP) and their phosphorylation by triggering oxidative stress (and, thus, fatty acid synthesis), and that this phenomenon is genotype-dependent (44). These properties, however, could be independent of lipid droplet binding.

The functional differences between genotype 1b and 3a core protein are likely related to amino acid sequence differences. The amino acid sequences of the two genotypes are very similar, likely owing to strong conservatory constraints on the 3D structure of the core protein, which is necessary to form mature nucleocapsids.

Single amino acid differences at the protein surface could modulate local folds, their stability and their interactions with other proteins. Core domain D2 has been implicated in lipid droplet association (35). Within this domain, three amino acid positions differ between genotype 1b and genotype 3a, namely L and V at position 144, V and I at position 162 and Y and F at position 164. These amino acid differences are not expected to modify the structure of this region but they could modulate its membrane-binding properties. Indeed, in genotype 1, V144 belongs to the hydrophobic loop that connects the two amphipathic helices interaction in-plane of the membrane interface, whereas L162 and F164 are involved in the last turn of helix II. A recent study has suggested that Y164F mutation of genotype 1a core protein leads to intracellular lipid accumulation (36). This mutation could increase the strength of helix II binding to the lipid droplet surface by eliminating the polar hydroxyl group of the tyrosine residue. In turn, the increased stability of the core-lipid droplet interaction could limit core protein degradation by the proteasome (34). F164 has also been implicated in the stronger FAS activation by genotype 3 core protein than by genotype 1 core protein despite similar localization of the two proteins at the lipid droplet surface (43).

Other amino acid differences between these two genotypes are found outside the D2 region. Our sequence analyses indeed revealed the hydrophobic nature of amino acids 4 and 16 in genotype 3a core proteins, while these positions are occupied by a polar residue (asparagine) in genotypes 1, 2, 4 and 5 (in genotype 6, position 4 is occupied by a leucine, a hydrophobic residue). These differences could alter local protein folding and stability, and also other protein interactions mediated by this region. The region located between amino acids 182 and 191 at the C-terminus of the core protein also exhibited numerous differences between genotypes 1b and

3a. Sequence differences in this area could modulate the kinetics of signal peptidase and signal peptide peptidase cleavage required for core protein maturation. We were not able, however, to identify precisely which amino acid difference(s) between genotypes 1b and 3a is (are) responsible for the observed functional differences.

Another important finding of this study is that the genotype 3a core protein-lipid droplet association is qualitatively and quantitatively independent of HCV-induced steatosis. In addition, alignment of quasispecies variants showed no difference according to steatosis; the only exception was at position 16, but the change was from a hydrophobic to a non-polar side-chain amino acid (valine to isoleucine), which is not expected to influence the protein fold. These results suggest that HCV genotype 3a infection is probably necessary but not sufficient to induce steatosis in patients with chronic HCV infection. They point to a role of other viral proteins, that could either act directly or modulate core protein function, and/or a role of host factors that would determine whether HCV genotype 3a replication in hepatocytes triggers the formation and growth of lipid droplets.

The host factors required for steatosis onset in HCV genotype 3a-infected patients are unknown. It has been shown that HCV core protein reduces the intra-hepatic activity of microsomal triglyceride transfer protein (MTP), an enzyme essential for hepatic lipoprotein assembly and secretion (45). Subsequent development of steatosis could vary according to polymorphisms of the apo AII gene (46, 47).

In conclusion, we show that the core protein of both HCV genotypes 1b and 3a binds tightly to the surface of intracellular lipid droplets. However, cells transfected with genotype 3a contain more neutral lipids in lipid droplets, and more large lipid droplets, than cells transfected with genotype 1b sequences. HCV core protein-lipid

droplet interaction could thus play a role in steatosis. Importantly, we found no genetic or functional differences between genotype 3a core proteins from patients with and without HCV-induced steatosis. This suggests that other viral proteins and/or host factors are involved in the development of hepatocellular steatosis in patients infected by HCV genotype 3a.

ACKNOWLEDGEMENTS

The data were obtained with the assistance of Daniel Stockholm from the Plateforme Génopôle (Evry, France) and Christo Christov from the Integrated Microscopy Core facility (Créteil, France). We are grateful to Jean-François Delagneau (Bio-Rad, France) for providing us with the Acap27 antibody.

REFERENCES

1. McCullough AJ. Obesity and its nurturing effect on hepatitis C. Hepatology 2003;38:557-559.
2. Hourigan LF, Macdonald GA, Purdie D, Whitehall VH, Shorthouse C, Clouston A, Powell EE. Fibrosis in chronic hepatitis C correlates significantly with body mass index and steatosis. Hepatology 1999;29:1215-1219.
3. Adinolfi LE, Gambardella M, Andreana A, Tripodi MF, Utili R, Ruggiero G. Steatosis accelerates the progression of liver damage of chronic hepatitis C patients and correlates with specific HCV genotype and visceral obesity. Hepatology 2001;33:1358-1364.
4. Westin J, Nordlinder H, Lagging M, Norkrans G, Wejstal R. Steatosis accelerates fibrosis development over time in hepatitis C virus genotype 3 infected patients. J Hepatol 2002;37:837-842.
5. Monto A, Alonzo J, Watson JJ, Grunfeld C, Wright TL. Steatosis in chronic hepatitis C: relative contributions of obesity, diabetes mellitus, and alcohol. Hepatology 2002;36:729-736.
6. Castera L, Pawlotsky JM, Dhumeaux D. Worsening of steatosis and fibrosis progression in hepatitis C. Gut 2003;52:1531.
7. Asselah T, Boyer N, Guimont M-C, Cazals-Hatem D, Tubach F, Nahon K, Daikha H, et al. Liver fibrosis is not associated with steatosis but with necroinflammation in French patients with chronic hepatitis C. Gut 2003;52:1638-1643.

8. Romero-Gomez M, Castellano-Megias VM, Grande L, Irles JA, Cruz M, Nogales MC, Alcon JC, et al. Serum leptin levels correlate with hepatic steatosis in chronic hepatitis C. Am J Gastroenterol 2003;98:1135-1141.

9. Rubbia-Brandt L, Fabris P, Paganin S, Leandro G, Male P-J, Giostra E, Carlotto A, et al. Steatosis affects chronic hepatitis C progression in a genotype specific way. Gut 2004;53:406-412.

10. Poynard T, Ratziu V, McHutchison J, Manns M, Goodman Z, Zeuzem S, Younossi Z, et al. Effect of treatment with peginterferon or interferon alfa-2b and ribavirin on steatosis in patients infected with hepatitis C. Hepatology 2003;38:75-85.

11. Patton HM, Patel K, Behling C, Bylund D, Blatt LM, Vallee M, Heaton S, et al. The impact of steatosis on disease progression and early and sustained treatment response in chronic hepatitis C patients. J Hepatol 2004;40:484-490.

12. Hui JM, Kench J, Farrell GC, Lin R, Samarasinghe D, Liddle C, Byth K, et al. Genotype-specific mechanisms for hepatic steatosis in chronic hepatitis C infection. J Gastroenterol Hepatol 2002;17:873-881.

13. Hezode C, Lonjon I, Roudot-Thoraval F, Pawlotsky JM, Zafrani ES, Dhumeaux D. Impact of moderate alcohol consumption on histological activity and fibrosis in patients with chronic hepatitis C, and specific influence of steatosis: a prospective study. Aliment Pharmacol Ther 2003;17:1031-1037.

14. Castera L, Hezode C, Roudot-Thoraval F, Lonjon I, Zafrani E-S, Pawlotsky JM, Dhumeaux D. Effect of antiviral treatment on evolution of liver steatosis in patients with chronic hepatitis C: indirect evidence of a role of hepatitis C virus genotype 3 in steatosis. Gut 2004;53:420-424.

15. Czaja AJ, Carpenter HA, Santrach PJ, Moore SB. Host- and disease-specific factors affecting steatosis in chronic hepatitis C. J Hepatol 1998;29:198-206.

16. Hwang SJ, Luo JC, Chu CW, Lai CR, Lu CL, Tsay SH, Wu JC, et al. Hepatic steatosis in chronic hepatitis C virus infection: prevalence and clinical correlation. J Gastroenterol Hepatol 2001;16:190-195.

17. Serfaty L, Poujol-Robert A, Carbonell N, Chazouilleres O, Poupon RE, Poupon R. Effect of the interaction between steatosis and alcohol intake on liver fibrosis progression in chronic hepatitis C. Am J Gastroenterol 2002;97:1807-1812.

18. Fartoux L, Poujol-Robert A, Guechot J, Wendum D, Poupon R, Serfaty L. Insulin resistance is a cause of steatosis and fibrosis progression in chronic hepatitis C. Gut 2005;54:1003-1008.

19. Cammà C, Di Marco V, Di Bona D, Rumi MG, Vinci M, Rebucci C, Cividini A, et al. Insulin resistance is associated with steatosis in nondiabetic patients with genotype 1 chronic hepatitis C. Hepatology 2006;43:64-71.

20. Rubbia-Brandt L, Quadri R, Abid K, Giostra E, Male PJ, Mentha G, Spahr L, et al. Hepatocyte steatosis is a cytopathic effect of hepatitis C virus genotype 3. J Hepatol 2000;33:106-115.

21. Rubbia-Brandt L, Leandro G, Spahr L, Giostra E, Quadri R, Male PJ, Negro F. Liver steatosis in chronic hepatitis C: a morphological sign suggesting infection with HCV genotype 3. Histopathology 2001;39:119-124.

22. Hezode C, Roudot-Thoraval F, Zafrani ES, Dhumeaux D, Pawlotsky JM. Different mechanisms of steatosis in hepatitis C virus genotypes 1 and 3 infections. J Viral Hepat 2004;11:455-458.

23. Barba G, Harper F, Harada T, Kohara M, Goulinet S, Matsuura Y, Eder G, et al. Hepatitis C virus core protein shows a cytoplasmic localization and associates to cellular lipid storage droplets. Proc Natl Acad Sci USA 1997;94:1200-1205.

24. Fujie H, Yotsuyanagi H, Moriya K, Shintani Y, Tsutsumi T, Takayama T, Makuuchi M, et al. Steatosis and intrahepatic hepatitis C virus in chronic hepatitis. J Med Virol 1999;59:141-145.

25. Shi ST, Polyak SJ, Tu H, Taylor DR, Gretch DR, Lai MM. Hepatitis C virus NS5A colocalizes with the core protein on lipid droplets and interacts with apolipoproteins. Virology 2002;292:198-210.

26. Abid K, Pazienza V, de Gottardi A, Rubbia-Brandt L, Conne B, Pugnale P, Rossi C, et al. An in vitro model of hepatitis C virus genotype 3a-associated triglycerides accumulation. J Hepatol 2005;42:744-751.

27. Moriya K, Yotsuyanagi H, Shintani Y, Fujie H, Ishibashi K, Matsuura Y, Miyamura T, et al. Hepatitis C virus core protein induces hepatic steatosis in transgenic mice. J Gen Virol 1997;78:1527-1531.

28. Moriya K, Fujie H, Shintani Y, Yotsuyanagi H, Tsutsumi T, Ishibashi K, Matsuura Y, et al. The core protein of hepatitis C virus induces hepatocellular carcinoma in transgenic mice. Nat Med 1998;4:1065-1067.

29. Lerat H, Honda M, Beard MR, Loesch K, Sun J, Yang Y, Okuda M, et al. Steatosis and liver cancer in transgenic mice expressing the structural and nonstructural proteins of hepatitis C virus. Gastroenterology 2002;122:352-365.

30. Perlemuter G, Letteron P, Carnot F, Zavala F, Pessayre D, Nalpas B, Brechot C. Alcohol and hepatitis C virus core protein additively increase lipid

peroxidation and synergistically trigger hepatic cytokine expression in a transgenic mouse model. J Hepatol 2003;39:1020-1027.

31. Moradpour D, Englert C, Wakita T, Wands JR. Characterization of cell lines allowing tightly regulated expression of hepatitis C virus core protein. Virology 1996;222:51-63.

32. Hope RG, Murphy DJ, McLauchlan J. The domains required to direct core proteins of hepatitis C virus and GB Virus-B to lipid droplets share common features with plant oleosin proteins. J Biol Chem 2002;277:4261-4270.

33. Murphy DJ. The biogenesis and functions of lipid bodies in animals, plants and microorganisms. Progr Lipid Res 2001;40:325-438.

34. Boulant S, Montserret R, Hope G, Ratinier M, Targett-Adams P, Lavergne J-P, Penin F, et al. Structural determinants that target the hepatitis C virus core protein to lipid droplets. J Biol Chem 2006:281:22236-22247.

35. Hope RG, McLauchlan J. Sequence motifs required for lipid droplet association and protein stability are unique to the hepatitis C virus core protein. J Gen Virol 2000;81:1913-1925.

36. Hourioux C, Patient R, Morin A, Blanchard E, Moreau A, Trassard S, Giraudeau B, et al. The genotype 3-specific hepatitis C virus core protein residue phenylalanine 164 increases steatosis in an in vitro cellular model. Gut 2007:56:1302-1308.

37. Hope RG, McElwee MJ, McLauchlan J. Efficient cleavage by signal peptide peptidase requires residues within the signal peptide between the core and E1 proteins of hepatitis C virus strain J1. J Gen Virol 2006;87:623-627.

38. Lindenbach BD, Evans MJ, Syder AJ, Wolk B, Tellinghuisen TL, Liu CC, Maruyama T, et al. Complete replication of hepatitis C virus in cell culture. Science 2005;309:623-626.

39. Wakita T, Pietschmann T, Kato T, Date T, Miyamoto M, Zhao Z, Murthy K, et al. Production of infectious hepatitis C virus in tissue culture from a cloned viral genome. Nat Med 2005;11:791-796.

40. Zhong J, Gastaminza P, Cheng G, Kapadia S, Kato T, Burton DR, Wieland SF, et al. Robust hepatitis C virus infection in vitro. Proc Natl Acad Sci USA 2005;102:9294-9299.

41. Rouille Y, Helle F, Delgrange D, Roingeard P, Voisset C, Blanchard E, Belouzard S, et al. Subcellular localization of hepatitis C virus structural proteins in a cell culture system that efficiently replicates the virus. J Virol 2006;80:2832-2841.

42. Shavinskaya A, Boulant S, Penin F, McLauchlan J, Bartenschlager R. The lipid droplet binding domain of hepatitis C virus core protein is a major determinant for efficient virus assembly. J Biol Chem 2007; in press.

43. Jackel-Cram C, Babiuk LA, Liu Q. Up-regulation of fatty acid synthase promoter by hepatitis C virus core protein: genotype-3a core has a stronger effect than genotype-1b core. J Hepatol 2007;46:997-1008.

44. Waris G, Felmlee DJ, Negro F, Siddiqui A. Hepatitis C virus induces proteolytic cleavage of sterol regulatory element binding proteins and stimulates their phosphorylation via oxidative stress. J Virol 2007;81:8122-8130.

45. Perlemuter G, Sabile A, Letteron P, Vona G, Topilco A, Chretien Y, Koike K, et al. Hepatitis C virus core protein inhibits microsomal triglyceride transfer

protein activity and very low density lipoprotein secretion: a model of viral-related steatosis. Faseb J 2002;16:185-194.

46. Kalopissis AD, Pastier D, Chambaz J. Apolipoprotein A-II: beyond genetic associations with lipid disorders and insulin resistance. Curr Opin Lipidol 2003;14:165-172.

47. Martin-Campos JM, Escola-Gil JC, Ribas V, Blanco-Vaca F. Apolipoprotein A-II, genetic variation on chromosome 1q21-q24, and disease susceptibility. Curr Opin Lipidol 2004;15:247-253.

FIGURE LEGENDS

Figure 1. (A) Alignment of the most frequent core-ΔE1 quasispecies variant sequences from each of the 8 patients infected by HCV genotype 1b or 3a, with (S) and without (NS) steatosis. The consensus of the 8 amino acid sequences (cons. seq.) is shown at the top. The residues at each position are indicated with the single-letter amino acid code. Amino acids identical to those in the consensus sequence are represented by a dot. The different regions of the constructs (HA tag, core, ΔE1, the residual multi-cloning site (MCS) and His6 tag) are represented by boxes. Dashes indicate deletions. **(B)** Repertoires of the amino acids observed in core region quasispecies from patients infected by HCV genotype 3a with (top) and without (bottom) steatosis. The amino acids are listed in decreasing order of observed frequency, from bottom to top for the patients with steatosis, and from top to bottom for those without steatosis. Each amino acid repertoire was deduced from the alignment of the quasispecies variant sequences within each class of patients. Amino acids observed only once are reported in lower-case letters. With the exception of position 16 (highlighted in gray), no differences were seen between patients with and without steatosis.

Figure 2. Analysis of core-ΔE1 processing by SPP. BHK C13 cells were transfected with plasmids encoding the different core-ΔE1 sequences, including pCΔE1-3a/1S, pCΔE1-3a/2S, pCΔE1-3a/3S, pCΔE1-3a/1NS, pCΔE1-3a/2NS, pCΔE1-1b/1NS, pCΔE1-1b/2NS, and pCΔE1-1b/3NS, as described in Materials and Methods. Cells were grown for 16 hours in the absence or in the presence of 100 μM $(Z\text{-}LL)_2$ ketone, an SPP inhibitor. Protein extracts from $(Z\text{-}LL)_2$ ketone-untreated and -treated

transfected cells were then subjected to western-blot analysis for core protein expression using an HRP-conjugated rat anti-HA MAb. In untreated cells (-), only the processed 21 kD form was present in all instances, whereas in $(Z\text{-}LL)_2$ ketone-treated cells (+), the uncleaved (23 kD) form of the core protein was also present.

Figure 3. Analysis of lipid droplet morphology in Huh-7 cells expressing HCV core protein. The cells were transfected with empty vector pHM6, pCΔE1-1b/1NS, pCΔE1-1b/2NS, pCΔE1-1b/3NS, pCΔE1-3a/1NS, pCΔE1-3a/2NS, pCΔE1-3a/1S, pCΔE1-3a/2S or pCΔE1-3a/3S, or infected with JFH1 virus, as described in Materials and Methods. Twenty-four hours post-transfection, the cells were fixed in paraformaldehyde and immunostained with mouse anti-core for 1 h at room temperature. After three washes in PBS the cells were incubated for 40 min with TRITC-conjugated goat anti-mouse IgG and BODIPY 493/503. The slides were mounted in fluorescent mounting medium containing DAPI. Images of 3D-reconstructed cells were generated by means of confocal laser microscopy from Z-stacks of serial confocal optical sections. The diameter of each lipid droplet contained in randomly selected control and transfected cells was determined. **(A)** Representative 3D reconstructions of cells expressing core protein from steatosis-free patients infected by HCV genotype 1b (1b), steatosis-free patients with genotype 3a infection (3a-NS), and patients with genotype 3a infection and HCV-induced steatosis (3a-S). The right panel shows a 3D reconstruction of JFH1-infected cells. Core protein, lipid droplets and nuclei are stained in red, green and blue, respectively. **(B)** Stacks of confocal images represented as volumes within a 3D-(xyz)-space using colored isosurface. A 3D-slicer script was used to obtain a section through lipid droplets (y axis), showing neutral lipids in green, HCV core protein in

red, and cell nuclei in blue. In the left-hand image, non-transfected Huh7 cells at the top exhibit numerous small lipid droplets. In genotype 3a-S core-transfected cells (bottom), large lipid droplets (green) are surrounded by HCV core protein (red). The right-hand image shows a higher magnification of another HCV genotype 3a-S core-transfected cell.

Figure 4. Lipid droplet morphological changes induced by HCV core protein expression. **(A)** Cumulative volume of lipid droplets per cell. The bar graphs represent the average amount of lipid droplet-associated neutral lipids per HCV genotype 3a-S core protein-expressing cell (dotted bar), per HCV genotype 3a-NS core protein-expressing cell (hatched bar), per HCV genotype 1b-NS core protein-expressing cell (gray bar), and per nontransfected control cell (white bar). Values are means ± SEM. **(B)** Proportion of lipid droplets > 6 μm diameter in cells expressing HCV genotype 3a-S core protein (dotted bars), HCV genotype 3a-NS core protein (hatched bars), HCV genotype 1b-NS core protein (gray bars), and in control Huh-7 cells (arbitrary value = 0). *p<0.001; **p<0.0001; NS, not significantly different.

Figure 5. Colocalization of HCV core protein and ADRP, a protein associated with the surface of lipid droplets. Core-ADRP colocalization was studied in Huh-7 cells expressing core-ΔE1 from patients infected by HCV genotype 1b without steatosis (panels A, D, G) and from patients with HCV genotype 3a infection with (panels C, F, I) and without steatosis (panels B, E, H). The cells were transfected with plasmids containing the different core protein sequences, fixed in paraformaldehyde after 24 h, and immunostained as described in Materials and Methods. Core protein appears red after Alexa 594 staining (panels A, B, C), and ADRP appears green after FITC

staining (panels D, E, F). The right-hand panels (G, H, I) show merged pictures of core protein and ADRP (and nuclear staining with DAPI).

Figure 6. Qualitative and quantitative analysis of HCV core protein-ADRP colocalization. Correlations between red pixels (core staining) and green pixels (ADRP staining) were calculated from several fields of confocal images of cells expressing genotype 1b, 3a-NS or 3a-S core protein. Panels A and B show representative results for cells expressing genotype 1b, 3a-NS and 3a-S core protein. The analyses were performed separately for large lipid droplets (diameter > 2.3 µm) **(A)** and small lipid droplets (diameter < 2.3 µm) **(B)**. In each panel, the field, the scatter plot (Pearson's analysis) and the cross correlation function (CCF, Van Steensel analysis) are shown from left to right. The calculated Pearson's coefficient (R) and the maximum CCF are indicated at the top of each scatter plot and CCF, respectively. The pixel shift (dx) value is indicated at the bottom of each CCF plot. **(C)** Pearson's coefficient (R-values) calculated for the different core protein sequences expressed in Huh7 cells (genotypes 1b, 3a-S and 3a-NS). Values for large (> 2.3 µm) lipid droplets are in dark gray, and values for small (≤ 2.3 µm) lipid droplets in light gray. Values are means ± SEM. The number of analyzed fields is indicated in each bar (*p<0.05; NS: not significant).

Table 1. Characteristics of the 8 patients selected for this study. The patients are identified by their HCV genotype (3a or 1b), followed by the patient number and the presence (S) or absence (NS) of virus-induced steatosis (example: 3a-1S is patient number 1 among the patients infected by genotype 3a with HCV-induced steatosis). NA: not applicable.

Patients	Gender	Age (years)	Genotype	Baseline HCV RNA level (log IU/ml)	Steatosis grade before therapy	Steatosis grade after therapy
3a-1S	M	29	3a	3.8	2	0
3a-2S	M	38	3a	5.9	3	1
3a-3S	M	29	3a	5.0	3	1
3a-1NS	M	47	3a	5.0	0	NA
3a-2NS	F	25	3a	4.1	0	NA
1b-1NS	M	32	1b	6.4	0	NA
1b-2NS	M	39	1b	6.7	0	NA
1b-3NS	F	61	1b	5.9	0	NA

Table 2. Primers and nested PCR conditions used to amplify the core-ΔE1 region.

		1st PCR round			2nd PCR round		
Genotype	**Amplified region**	**Primer name and sequence**	**Cycles**		**Primer name and sequence**	**Cycles**	
3a	Core-ΔE1	**CORE SE** GTAGTGTTGGGTCGCGAAAGG **CE1.ASE.3a** GCCCCGGCTATTATGTC	95°C 30 s 60°C 30 s 70°C 120 s	X 30	**Core.Man.pHM6.S** GACGAAGCTTACGCAGCACACTTCCTAAACCTC **CE1.ASi.3a.EcoRI** CATGGAATTCACGTCCATCATATCCCAAGCCATTCG	95°C 30 s 61°C 30 s 70°C 120 s	X 30
1b	Core-ΔE1	**CORE SE** GTAGTGTTGGGTCGCGAAAGG **CE1.ASE.1b** GCTTGTGGGATCCGGAGTAACTG	95°C 30 s 60°C 30 s 70°C 90 s	X 30	**Core.NM.pHM6.S** GACGAAGCTTACGCAGCACGAATCCTAAACCTC **CE1.ASi.1b.EcoRI** CATGGAATTCACGTCGTTCATACATCATATCCCAAGC	95°C 30 s 61°C 30 s 70°C 120 s	X 30

Figure 1A

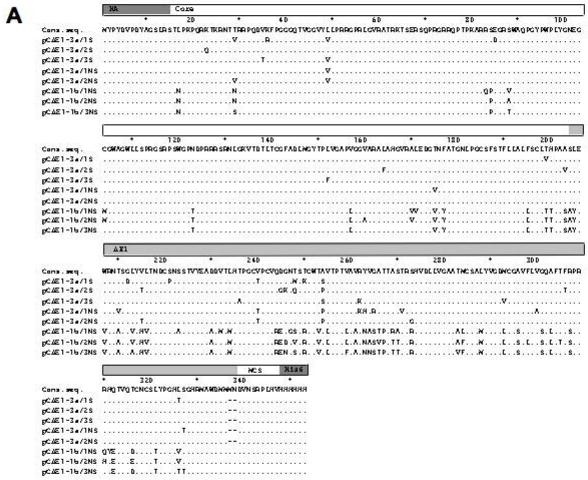

Figure 1B

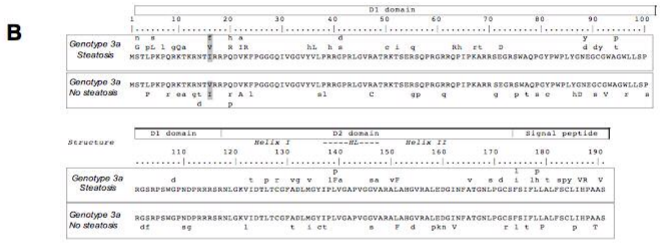

Figure 2

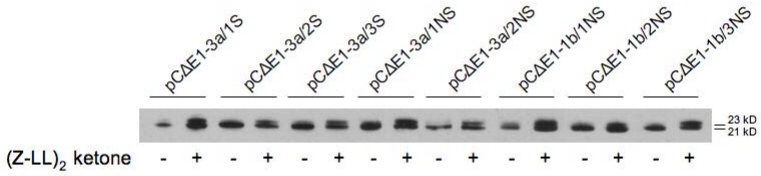

Figure 3A

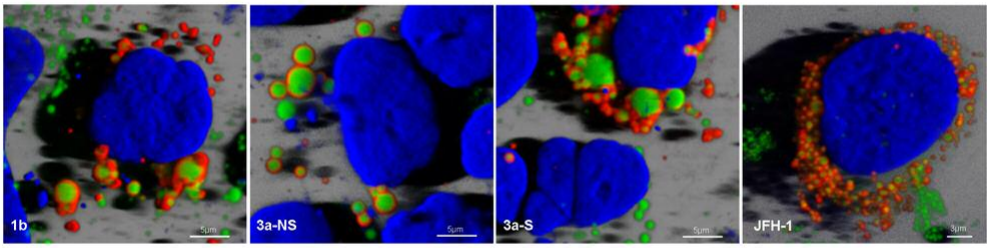

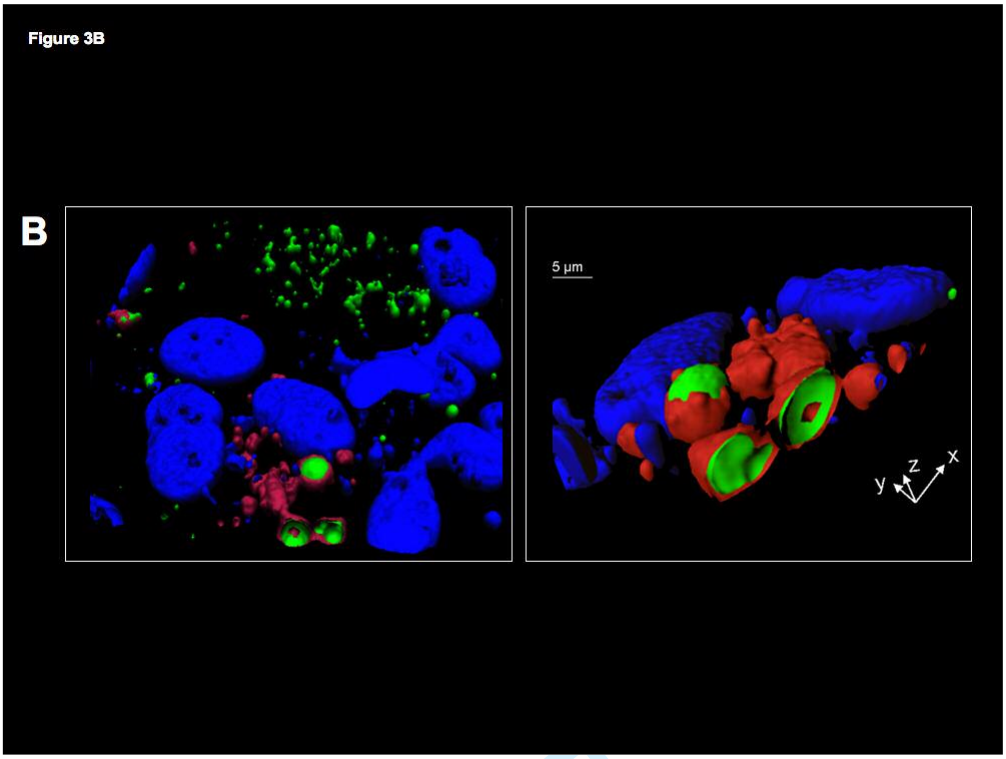

Figure 4

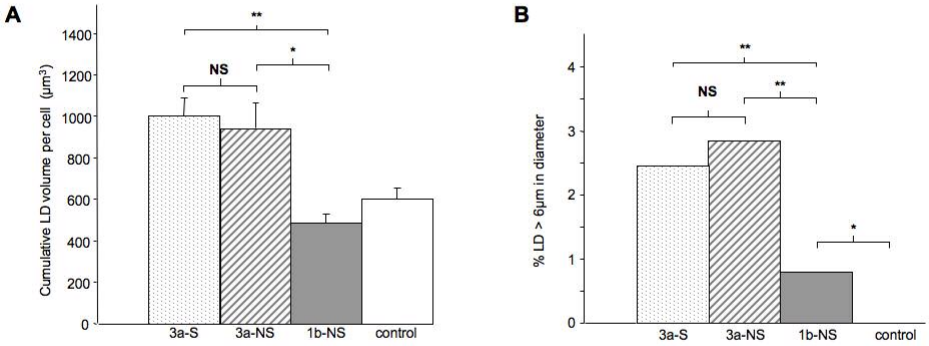

Figure 5

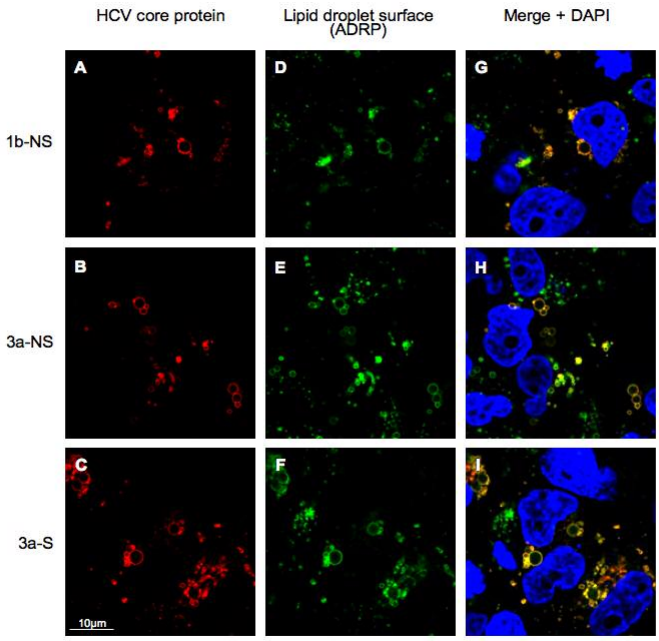

Figure 6